

# AUTOMATIC SEGMENTATION OF THE LUMEN OF THE CAROTID ARTERY IN ULTRASOUND B-MODE IMAGES USING FUZZY LOGIC CLASSIFIER

D.SASIKALA<sup>1</sup> B.NANDHINI<sup>2</sup> M.NARGEESH BANU<sup>3</sup>

A.NIVETHA<sup>4</sup> R.SOWMIYA<sup>5</sup>

<sup>1</sup>Professor/ECE , Vivekanandha College of Engineering for Women, Tamilnadu,India

<sup>2,3,4</sup>M.E VLSI design, Vivekanandha College of Engineering for Women,  
Tamilnadu,India

<sup>5</sup>M.E Applied Electronics, Vivekanandha College of Engineering for Women,  
Tamilnadu,India

## Abstract:

*In this paper, the new method is proposed for recognizing B-mode ultrasound (US) imaging of common carotid artery (CCA) in longitude. Automatic segmentation of the arterial lumen from ultrasound images is an important task in clinical diagnosis. Carotid artery recognition, the first task in lumen segmentation, should be performed in a fully automated, fast, and reliable way to further facilitate the low-level task of arterial delineation. In this paper, a user-independent, real-time algorithm is introduced for carotid artery localization in longitudinal B-mode ultrasound images. The proposed method has four major steps. The process starts with image area selection, vertical intensity profile (VIP) signal selection, lumen center point detection; the proposed method classifies center points using fuzzy logic classifier. This provides a medial axis with efficient lumen recognition data. The data sets used included 2,149 images from 100 subjects taken from three different institutions and covering a wide range of possible lumen and surrounding tissue representations. Using the optimized values, the carotid artery was recognized in all the processed images in both multi-frame and single-frame data. Thus, the introduced technique will further reinforce*

*automatic segmentation in longitudinal B-mode ultrasound images.*

**Index Terms**—Lumen recognition, carotid artery, segmentation, ultrasound, fuzzy logic

## I.INTRODUCTION

The common carotid artery (CCA) is the artery that supplies the human head, specifically the front part of the brain and neck, with oxygenated blood. Like other arteries, it is known for its paired structure: one for left part (with origin in the aortic arch) and another one for the right part of the human body (with origin in the neck). Vascular non-invasive ultrasound (US) allows the estimation of morphological and dynamic parameters of arteries, such as diameter and distension (Reneman et al., 2005) or intima-media thickness (IMT) (Van Bortel et al., 2001). To perform these measurements fast, accurately and reliably with minimal inter and intra-user variability, the segmentation of the underlying ultrasound image should be computerized.

Image segmentation may be thought as consisting of two related processes (Udupa et al., 2006): recognition, i.e. the high level task of determining roughly where a specific structure is located, and delineation, i.e. the low level task of determining the precise spatial extent of such structure. The topic of this paper concerns CA recognition through lumen medial axis detection.

So far, the various methods are introduced for CA segmentation requires manual user assistance in arterial lumen recognition (see [5]–[9]). few algorithms offer full automation in CA segmentation (see [16],[2],[3]). The user-induced artifacts were limited by completely automated CA recognition [1], thus providing (i) better accuracy in recognizing the random-shaped arterial lumen and (ii) repeatability, whereas it provides (iii) increased productivity compared to the manual one. Moreover, focusing on recognition alone, which remains the most challenging task in image segmentation, may also (iv) improve overall segmentation accuracy by facilitating the measurement procedure [1], (v) reduce overall computational cost, (vi) provide better flexibility, and (vii) offer better error control, because it is evaluated independently.

## II. RELATED WORK

To our knowledge, previous work focused solely on automatic arterial recognition in longitudinal B-mode images is relatively limited compared to the work on CA delineation. Delsanto et al. [14] introduced an automatic region of interest (ROI) identification approach as initialization for a user-independent segmentation algorithm. However, the proposed algorithm may be deceived by wall calcium plaque presence, and it is not well-suited for real-time applications. Rossi et al. [1] developed a real-time algorithm for the automatic recognition of the common Carotid Artery (CCA) that acts directly on the envelopes of received radio frequency echo signals.

However, their method can be exploited to its full extent when applied to multi-frame data. Wan et al. [15] suggested two different methods for CCA recognition; a single-frame, and a multi-frame approach. However, both their methods are also prone to low Signal-to-Noise Ratio (SNR) in the lumen and to jugular vein presence. Benes et al. [19] proposed an automatic CA localization approach based on a support vector machine (SVM) classifier and a novel random sample consensus (RANSAC) method [18] to suppress misclassified points. However, their approach is not

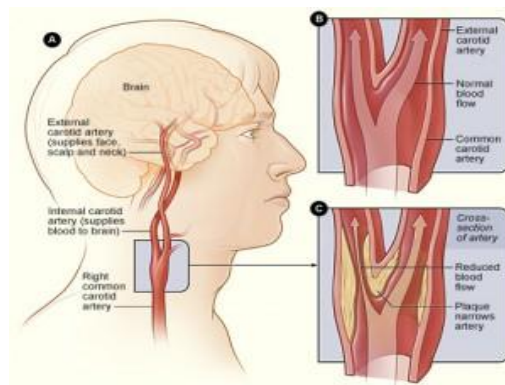
appropriate for real-time applications. Emmanouil G. Sifakis et al. [4] proposed carotid artery recognition based on Vertical intensity profile (VIP) for medial axis formation in lumen. The drawback of this method uses a basic classification for CA recognition.

The main aim of this paper was to develop a fully automated and real time technique for CA recognition in longitudinal B-mode ultrasound images. The method operates efficiently on a single ultrasound image without the need of utilizing any subsequent frame information. Our CA Recognition approach based on a Fuzzy logic classifier to suppress misclassified points. It was also systematically compared on an equal footing with another, promising method for CCA localization.

## III. MATERIALS AND METHODS

### A. Image Datasets

In this study, a total of 2,149 longitudinal B-mode ultrasound images of the CA recorded from 100 subjects, and collected from three separate datasets namely St. Mary's Hospital Dataset (SMH), Aretaieion University Hospital Dataset (AUH), SPLab Dataset (SPL) were used for performance evaluation of the proposed algorithm. Fig. 1 shows a simple CCA and Fig 2 shows longitudinal B-mode ultrasound image example of the tested ultrasound images. All images are depicting CCA in longitudinal scan of



different volunteers.

**Fig 1. Diagram of common carotid artery wall**

The images were scanned with different settings of acquisition hardware (frequency, depth, gain) and different positioning of a probe. The images cover a wide spectrum of (i) CA sites (e.g. common, internal, external, bulb), (ii) subject profiles (e.g. age, sex, weight), and (iii) clinical conditions, and they were acquired using different (iv) ultrasound image acquisition systems and linear array transducers, (v) sonographers, and (vi) settings (e.g. depth, gain, time gain compensation (TGC)).

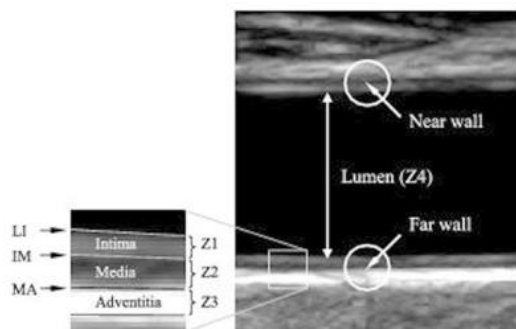


**Fig 2. Longitudinal B-mode ultrasound image of common carotid artery with layer description. The lumen is the region where the blood flows**

## B. Algorithm Architecture

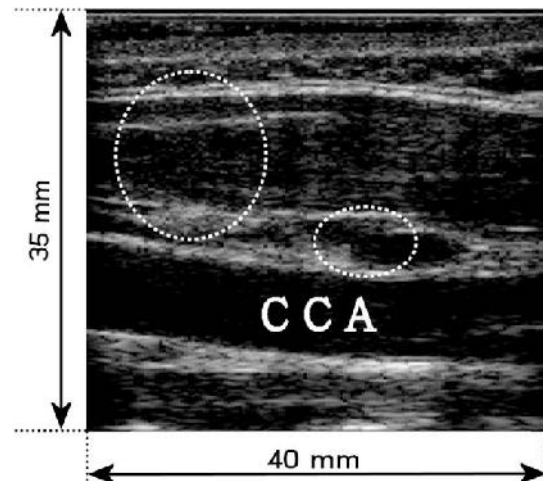
The overview of the proposed algorithm, which was developed and evaluated within Matlab® 7.9 R2009b (The MathWorks Inc., Natick, MA, USA), is shown in Fig. 3. Briefly, a finite number of equally spaced, vertical intensity profiles (VIP) is considered in a single image. For every VIP signal, a statistics-based procedure is used for a single lumen center point identification. Then, a subset of the resulting lumen center points, designated as the 'backbone', is further processed to accurately estimate the CA lumen position.

### 1) Image Area Selection

In US longitudinal scans, the CCA appears as a structure oriented in horizontal direction, often covering the entire frame width. In the vertical dimension of the US frame, the artery is usually located at depths between 10 and 30 mm with a diameter between 4 and 9 mm, depending on age and sex of the subject. The artery structure appears

as a region having very low echogenicity (the lumen) surrounded by two bright bands (the arterial walls). The lumen center position may vary over the frame, consistent with a curved or inclined artery or with local narrowing's of the lumen due to a stenosis.

A vascular US image may contain many patterns mimicking the appearance of an artery of



interest, e.g. actual tissue structures, artifacts, reverberations and other vessels (Fig. 3). The upper

**Fig 3. Ultrasound B-mode image of the common carotid artery (CCA).**

part of each frame (the first 2–3 mm) contains particulars that are of no interest for the lumen localization task (the gel skin interface for instance). Moreover, users often tend to have the region of interest in the center of the image. Therefore, we ignore the information contained in the upper 3 mm and in the lateral 4 mm on each side (10% of the image width), whereas preserving the entire image height.

### 2) VIP Signal Selection

In the reduced image, the concept of lateral interspacing adapted by Rossi et al. [1] for vertical signal selection [3], [1], [14] was followed. Specifically, a finite number ( $N$ ) of VIP signals was considered every  $S_{step}$  mm (Fig. 4(b)), thus reducing its 2D information content to a series of 1D signals. The lateral interspacing of  $S_{step}=0.5$  mm was selected, because it provides a rather adequate sample size for robust and accurate CA recognition, and has a step relatively low

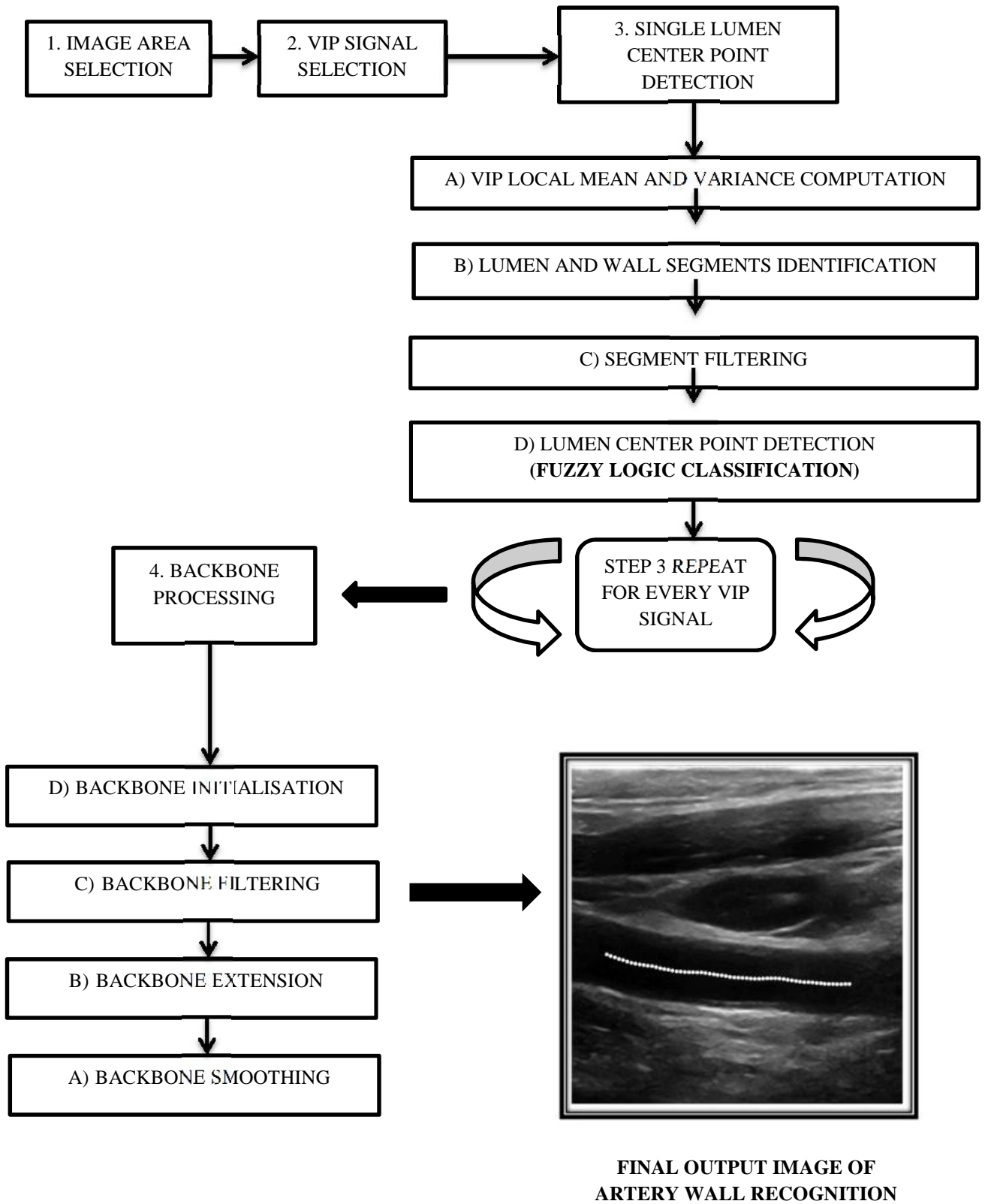


**Fig 4 Block diagram of proposed system**

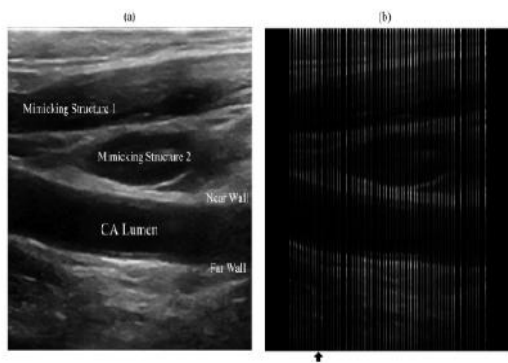


**Fig 5. VIP signal selection with  $swl=0.5$ , arrow indicates 10<sup>th</sup> VIP signal from left.**

computational cost. After testing, any value of  $S_{step}$  in the interval (0 0.5] mm yielded the same success rate, while smaller values were only at the expense of increased computational cost.

### 3) Single Lumen Center Point Detection:

For each selected VIP signal (Fig. 4(b)), a statistics-based, multistep procedure was used for the estimation of a single lumen center point. The CA anatomical characteristics were used for this its process from the bottom of the image and moving upwards, first one ordinarily encounters the procedure. In particular, the ultrasound image starts (usually brightest) far wall region, then the (usually darkest) lumen, and then the (usually second brightest) near wall.

The proposed procedure consists of the following sequential steps:

### 3.1 VIP local mean and variance computation

During this step, a sliding window of fixed length  $swl$  is used to calculate the smoothed local mean and variance of the VIP signal. The selection of

$swl$  is a result of a trade-off between including a relatively large number of intensity points to improve the estimated statistics, and following the intensity-dependent ‘steepness’ observed close to the lumen borders more effectively. The length of  $swl = 0.5$  mm was initially selected, equal to half of the mean adventitia thickness [18], i.e. accounting also for extreme cases where only the adventitia appears bright in the ultrasound image, while the other layers appear dark.

### 3.2 Potential lumen and wall segments identification

This step is followed to identify ROIs belonging to the vessel lumen, and ROIs belonging to the vessel wall. This approach divides the distributions of the local mean and variance vertical intensities using percentile-based thresholds to recognize the potential corresponding ROIs. Thus, because vessel lumen pixels typically have low mean intensities and low variances. The VIP signal’s potential vessel lumen segments are selected only if local mean intensity ( $L_{Loc} =$  lower 25<sup>th</sup> percentile), and, at the same time, (ii) local variance intensity distribution ( $L_{disp} =$  lower 25<sup>th</sup> percentile).

Similarly, because vessel wall pixels should have relatively high mean intensities, a VIP signal’s segment is considered as possibly belonging to the vessel wall if its corresponding local mean intensity distribution belongs to its upper quartile ( $W_{loc} =$  75th percentile).

Fig. 6(a) shows the potential lumen and wall segments superimposed on the original ultrasound image.

### 3.3 Segment filtering

The identified lumen and wall segments proceeds with two cascade routines of filtering. The first one fills the small gaps between two consecutive segments. The second one discards short length segments. Thus, at the beginning, the distance between two consecutive segments is calculated and if it is found lowers than a user-defined distance threshold, the two segments are merged into a single segment. Subsequently, segments shorter than a user-specified threshold are rejected.

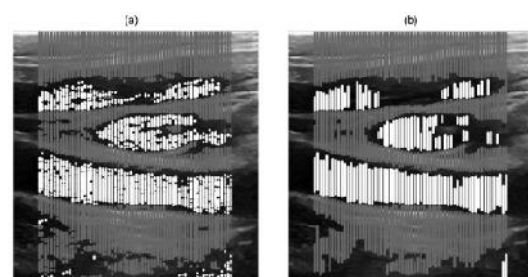


**Fig 6(a) lumen and wall segments identified output (b) Segment filtered image**

T

The four cut-offs for the lumen and wall segments, namely the two distance thresholds ( $L_{fillgap}$  and  $W_{fillgap}$ ) and the two length thresholds ( $L_{minlength}$  and  $W_{fillgap}$ ), are selected considering (i) that the mean adventitial thickness is about 1 mm [18], and (ii) two worse-case scenarios. The adventitia (of either the near, or the far wall) appears bright in the ultrasound image, while the other layers of the vessel wall appear dark; appear dark; that is, they cannot be discriminated from background (e.g. blood).

In this extreme case, two consecutive segments possibly belonging to the vessel lumen should be merged only if their distance is not greater than the adventitial thickness. Thus, the minimum distance threshold for the lumen segments  $L_{fillgap}$  should be equal to 1 mm. potential wall segments should have minimum length equal to the adventitial thickness; thus, the length threshold for the wall segments  $W_{minlength}$  was also set equal to 1 mm. In the other worse-case scenario, the vessel lumen is heavily occluded such that the lumen diameter locally becomes very small. Defining this minimum lumen diameter as 1 mm, the two remaining cut-offs may be set in a similar manner. Specifically, two consecutive segments possibly belonging to the vessel wall should be merged only if their distance is not greater than the lumen diameter. Thus, the minimum distance threshold for the wall segments  $W_{fillgap}$  should be equal to 1 mm. Furthermore, the potential lumen segments should have minimum length equal to the minimum lumen diameter; thus, the length threshold for the lumen segments  $L_{minlength}$  was also set equal to 1 mm. Accordingly,  $W_{minlength} = L_{fillgap}$  and  $L_{minlength} = W_{fillgap}$ .

Fig. 6(b) illustrates the filtered potential lumen and wall segments superimposed on the original ultrasound image.

### 3.4 Potential lumen center point identification

To automatically identify the VIP signal's potential lumen center point, a heuristic search of fuzzy logic classifier [23] is applied to the filtered lumen and wall segments. In particular, the VIP signal is searched for (i) the first wall-lumen segment pair starting from the bottom of the image (Group U), or, instead, for (ii) the last wall-lumen segment pair starts from the top of the image (Group D). To facilitate the classifier, the midpoint

of each line segment is taken as its representative. Thus, at the end of the procedure the output would be a single potential lumen center point for each VIP signal. Each point is resulted either from Group U or Group D (or none of them), and thus it is designated accordingly.

Fig.7(a) shows the output of this step for a low-quality ultrasound image.

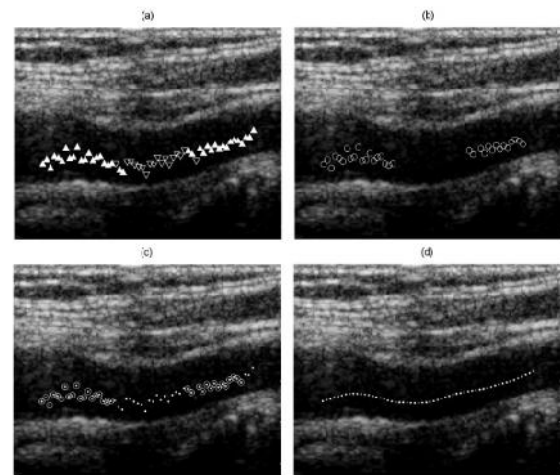


**Fig 7(a) Lumen center point detection output, where a potential point is selected for each corresponding VIP signal. Each point belongs either to Group U (upward pointing triangles), or to Group D (downward pointing triangles). The backbone is initialized as the subset of Group U points (appearing as white-filled, upward-pointing triangles). (b) Backbone filtering output. (c) Backbone extension output (circles indicate the filtered, while dots the extended points). (d) Backbone smoothing output.**

### Fuzzy Classifier

The classification was performed on the basis of image local features obtained from a neighborhood of particular pixels. The appropriate selection of features is crucial for the performance of the classifier.[23] It is important to select features that separate both classes. In this implementation, appropriate features were selected according to our local mean and variance of VIP signal.

### 4) Backbone Processing

At the end of the application of the lumen center point detection algorithm to all VIP signals,

a number of Group U and/or Group D points that equals or is smaller than  $N$  is generated.[4] However, due either to artifacts in some VIP signals, or to the impossibility to find segments/points meeting the imposed constraints, the resulting set of points needs to be further processed to substantially increase the success rate. Therefore, another multi-step procedure is followed, the input of which consists of a subset of these points. This subset of points, designated as the 'backbone', is suitably initialized, filtered, extended and smoothed, so as to extract a robust and accurate arterial lumen center representation. More specifically:

#### 4.1 Backbone initialization

Because the far wall region appears typically brighter than the near wall [21], points belonging to Group U are considered with higher confidence than those belonging to Group D. Hence, the backbone is initialized as the Group U points. However, Group D points are also preserved for potential usage in the backbone extension step described below.

#### 4.2 Backbone filtering

The initial backbone needs to be filtered for outliers. However, this is an extremely challenging task, due to the fact that the CA can be slightly inclined and/or curved within the image, which implies variations in the lumen center position over the image. These variations, which correspond to true lumen points, cannot be easily discriminated from outliers.

To overcome this, a two-stage procedure is introduced that comprises an adaptive filtering that becomes more severe in more ambiguous cases (i.e. in cases where backbone points are very disperse) gradually. The goal of the proposed approach is to output a filtered backbone that consists solely of true lumen estimates. Apparently, this also comes at the expense of discarding a few or a relatively larger number of true lumen center points, too (in particular, the more disperse the backbone points are, i.e. the more inclined and/or curved the lumen is, the more true backbone points will be eliminated). However, to compensate for this effect, a heuristic backbone expansion algorithm is applied afterwards (see, the following step).

In ultrasound longitudinal images, it is quite common to encounter CA-mimicking patterns, which (i) appear in a different depth range, and (ii) are usually more localized, spanning a smaller part of the image width (Fig. 4(a)). Therefore, most of the CA center points are distributed around a specific depth level, which is also different from that of all other vessel-like structures' center points.

Based on the hypothesis that the majority of the true backbone points is located in a similar depth within the ultrasound image [1], the two-stage filtering algorithm considers the distribution of the initial backbone's y-coordinates (depth values), along with its initial mean and standard deviation (SD). At the first stage, points with y-values greater than  $f_{SD0} = 1.5 SD$  from the mean (a common selection for filtering outliers in statistics) are identified and excluded.

If the initial backbone points are highly disperse, i.e. the initial SD exceeds a maximum acceptance threshold, the process is repeated until convergence. At the second stage, the new distribution of points is calculated, along with its new mean and SD. In the case where the new SD exceeds a maximum acceptance threshold, i.e. the filtered points are still highly disperse, the first stage is repeated until convergence, however, this time a new SD is computed and the initial threshold of  $f_{SD0} = 1.5 SD$  is reduced by  $f_{SDstep} = 0.1 SD$  at the end of every cycle (any value of  $f_{SDstep}$  in the range [0.05 0.5] does not significantly affect the algorithm's final success rate). The second process is repeated until SD does not exceed the maximum acceptance threshold anymore. Thus, the more scattered the new point distribution, the more severe the filtering.

To select an appropriate value for the maximum acceptance threshold used in both filtering stages, the probability density function (pdf) of SD was estimated. Particularly, the pdf of the initial backbone points' SD (initial SD) of  $\sim 10^3$  ultrasound images was estimated using a Gaussian kernel density estimator [11]. The image set used for the pdf estimation of SD included images from all the datasets to ensure a wide range of possible SD values. Specifically, we included all the images from datasets AUH and SPL, and 10 recordings from dataset SMH (5 healthy young, 2 healthy elderly, and 3 stenotic subjects).

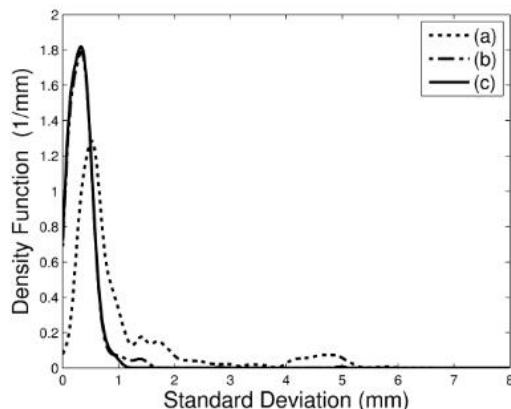


**Fig. 8.** Probability density function of SD of (a) the initial backbone (light gray, dotted line), (b) the output backbone at the end of filtering stage 1 (dark gray, dash-dotted line), and (c) the output backbone at the end of filtering stage 2 (black, solid line), resulting from a non-parametric kernel density estimation, and using a maximum acceptance threshold of 1.

As illustrated in Fig. 8(a), the probability of the initial SD to fall within region (0, 1) is relatively higher than to take on values that exceed the upper limit of that range. The higher SD values correspond to more dispersed backbone point distributions that may result either from a relatively large number of false-positive points, or from a highly inclined and/or curved CA. Therefore, the value of  $f_{\max SD} = 1\text{mm}$  was chosen for the maximum acceptance threshold (any value smaller than the selected one does not significantly alter the algorithm's final success rate). Fig. 8(b), (c) show the SD's pdf estimates at the end of filtering stages 1 and 2, respectively.

The filtered backbone of the low-quality image is shown in Fig. 7(b).

#### 4.3 Backbone extension

During this step, a heuristic extension algorithm is applied with the purpose of either (i) correcting/tuning the backbone initialization step, thus accounting for cases where part(s) of the initial backbone is missing (resulting from e.g. low-quality images with far wall part(s) appearing faint, as in Fig. 7(a)), or (ii) expanding the severely filtered backbone, thus accounting for a potential true backbone point(s) elimination (resulting from ambiguous cases, e.g. due to high lumen inclination and/or presence of CA mimicking structure(s)).

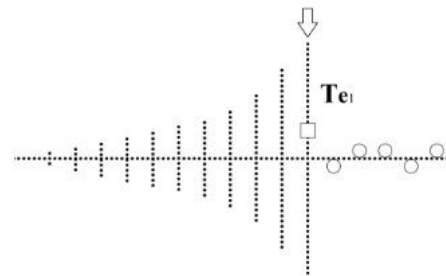


**Fig.9.** Example of the background extension algorithm concept. The circles correspond to a filtered backbone left end, while the horizontal line to its local depth level. The arrow indicates the VIP position where the discontinuity begins, thus the search initiation for potentially filtered out backbone points. For this first VIP position, a candidate point should be located within the range indicated by the vertical line, i.e. should be maximum up to  $Te_1$  mm distant from the local depth level. If this is not the case, the search moves to the next VIP position, and so on (until a maximum number of 20% of N), each time using an exponentially decreasing threshold  $Te$ . The vertical lines, formulating a discrete funnel-like area, represent this new point's search range. In this example, the new point is located within the range of the first VIP position (indicated by the square), thus it is included in the backbone extension set. The same procedure is initiated for all the neighboring VIP positions, until no more new points enter the backbone.

More specifically, given the existence of at least one discontinuity (void) in the output of the backbone filtering procedure (created after the backbone initialization and/or filtering steps, as in Fig. 7(b)), at the left and/or the right of every filtered backbone end, the superset of the corresponding Group U and Group D points is searched for a potential neighboring lumen center point. To specify this 'adjacency', firstly, a corresponding small window of fixed length  $xw_l$  (equals 10% of N) is applied at the vicinity of the backbone end, and a local depth level value is determined. The latter is defined as the mean of the depth values of all the filtered backbone points located within the specified window. Then, the potential neighboring point is included in the extended backbone, only if its distance from the local depth level is smaller than a step-wisely

decreasing threshold  $T_e$ , which is initialized with the maximum value of 2 mm.

In particular, if the candidate lumen point is not located within the initial value of  $T_{e1} = 2$  mm from the local depth level (in the y direction), the algorithm searches for the next candidate point at the next VIP position, and so on (within an interval that equals 20% of N in the x direction), each time using the exponentially decreased value of  $T_e$  ( $T_e(n) = T_{e1} \cdot e^{-\lambda(n-1)}$ ,  $n=1, \dots, \sim 0.2N$ ) and a decay constant of  $\lambda = 5$  (even though parameters  $x_{wl}$  and  $T_e$  should be kept relatively small and parameter  $\lambda$  relatively large, the algorithm's final success rate is not significantly affected over a broad range of their corresponding values).

An exponential decrease with a relatively large decay constant was preferred over e.g. a linear decrease in order to be more stringent, and hence minimize the potential of false positive points inclusion. Thus, a discrete funnel-like search area is formulated within which a potential backbone extension point should be located (Fig. 9). The procedure is repeated for each 'missing' backbone point, calculating an updated local depth level each time a new point enters the backbone. The backbone extension algorithm output is illustrated in Fig. 7(c).

#### 4.4 Backbone smoothing:

As a final step, the extended backbone is further smoothed to account for potential spike points, emanating e.g. due to speckle content and/or localized artifacts. To smooth the backbone without altering its local traits, the locally weighted least squares regression loess method was applied, using a 1st degree polynomial model and a smoothing window  $mwl$  equal to 20%. Any value for  $mwl$  in the range [10 30] % could be used. However, it is recommended not very large values (e.g.  $mwl$  40%) to be used in order not to alter the natural curvature of the identified backbone.

The final result of the automated CA recognition algorithm is illustrated in Fig. 7(d).

## IV RESULTS

To validate our algorithm, as well as to fine tune some of its preselected parameters, a procedure based on 3-fold cross-validation was performed. Specifically, completely independent

image sets were used for (i) parameter tuning, and (ii) testing and evaluating the proposed method. Moreover, instead of segmenting the original dataset, another initial image set was formed that contained the complete AUH and SPL datasets, and only the first frame of each recording of the SMH dataset, in order to eliminate any potential favorable bias during the different subset formation. This dataset was first partitioned into three nearly equally sized subsets. Subsequently, three iterations of parameter tuning and evaluation

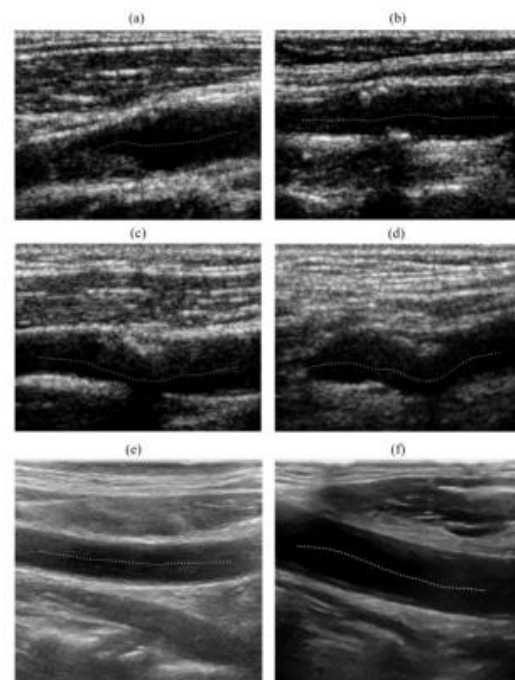


**Fig. 10. Demonstration of the robust nature of the proposed CA recognition algorithm (a)-(d) in very low-quality B-mode images from the SMH dataset and the AUH dataset.**

were performed such that within each iteration a different subset of the data was held-out for algorithm's testing and evaluation (testing set), while the remaining two subsets were used for algorithm parameter tuning (training set).

In each task (parameter tuning and evaluation), the automatic CA recognition outputs were compared with semiautomatic lumen center delineations made by an expert sonographer. Specifically, for an image, the user manually identified (i) the intima-lumen interface of the near

wall and (ii) the lumen-intima interface of the far wall, from where the reference arterial centerline was computed.

The semi-automatic delineation was performed on each image for the AUH and SPL datasets, and on the first image of each sequence for the SMH dataset. For the rest of the images in the sequence, the two aforementioned interfaces were automatically tracked using the adaptive block matching technique ABM\_FIRF2, described in detail in [22]. The algorithm's automatic CA recognition output was considered correct if it did not deviate more than 2 mm from the reference tracing [3], [1].

To rate the results of the automatic CA recognition, three performance metrics were considered, namely (i) the success rate SR (%), which indicates the success percentage in the total number of images in the set, (ii) the mean frame coverage FC(%), which is expressed by the ratio of the distance between the outermost VIP signals with a correctly identified centerline and the resized image width [1], and (iii) the mean distance D (mm) between the automatic and the reference centerline position. The mean FC and D values were derived after averaging over all the processed images.

The algorithmic parameters that were selected from tuning results shown in [4]. The optimized values of the tuned algorithm's parameters overall are  $(swl, L_{disp}, L_{loc}, W_{loc}) = (0.5 \text{ mm}, 25\text{th}, 50\text{th}, 75\text{th})$ .

Fig. 10 shows some automatic lumen recognition examples using the above optimized parameter values.

## V. DISCUSSION

In this study, a novel algorithm was introduced for the automatic recognition of the CA in longitudinal B-mode ultrasound images. The proposed algorithm consists of multiple cascaded steps with fuzzy logic classifier and exploits basic statistics along with arterial anatomical knowledge. The validity of the technique was investigated by direct comparison with expert's results over a completely diverse dataset range on a 3-fold cross validation basis. Through this process (training phase), a fixed optimized parameter set was

derived, capable of successfully localizing CA with full automation in a wide range of possible arterial representations.

The developed method performed very effectively and successfully localizes the CA based on a low computational complexity algorithm, whereas operating directly on the raw image, e.g. without the need of any time consuming 2D image processing techniques. wide range of parameter value combinations.

Furthermore, the examples of Fig. 10 illustrate the algorithm's effectiveness using the same optimized thresholds in images (i) of poor quality (ii) with atherosclerotic plaques, (iii) with CA-mimicking structures appearing above and/or below the CA, (iv) with relatively high and/or varying luminal gray level, and (v) with different arterial inclinations and/or curvatures. All of the above indicate the high performance and high robustness of the introduced approach and its tolerance parameterization.

The algorithm was designed based mainly on the fact that the arterial lumen has (i) lower mean intensity and lower variance (apart from the adventitia layer) compared to its surroundings, and (ii) a smoothly curved shape. In some images, a relatively low FC was observed, probably due to a combination of more than two of the following factors: (i) a high (and/or variant) luminal intensity, (ii) CA mimicking structure presence covering a significant part of the entire image width (especially below the CA), (iii) a poor far wall representation, and (iv) an abruptly curved arterial shape (e.g. due to a relatively large plaque). In these cases, a certain percentage of backbone points was missing (discarded during the backbone filtering step), resulting in a shorter final backbone (e.g. Fig. 10(a)).

Furthermore, in cases of non-uniform luminal intensity, caused e.g. by high speckle content and/or artifacts residing within the arterial lumen, the backbone appeared slightly affected. Also, the algorithm may not be able to distinguish between lumen and hypo echoic tissue, e.g. when increased speckle content and/or a highly stenotic hypo echoic plaque are present, which is generally believed to be associated with soft and unstable tissue. These limitations, however, are considered of minor significance, in the context of this study,

given that the purpose of the suggested methodology was the unambiguous identification of a ROI that includes the CA [1]; objective which is fulfilled.

## VI CONCLUSION

In summary, the algorithm described in this paper provides a simple, fast, robust and highly efficient way to locate the CA in longitudinal B-mode ultrasound images. Applied directly to the raw image, it managed to recognize the CA with high robustness and reliability. Moreover, the method's particularly low computational cost, its single frame sufficiency, along with its extendibility, facilitates both a wider range of on-line and off-line applications. All these render the introduced technique a suitable and reliable tool for lumen recognition that will further reinforce the completely user independent segmentation of the CA in longitudinal B-mode ultrasound images.

## ACKNOWLEDGEMENT

This work is supported by St. Mary's Hospital, London, UK, for the recording of the SMH dataset and also for the University of Athens, Aretaieion Hospital for helping in the AUH data collection.

## REFERENCES

- [1] A. C. Rossi, P. J. Brands, and A. P. G. Hoeks, "Automatic recognition of the common carotid artery in longitudinal ultrasound B-mode scans," *Med. Image Anal.*, vol. 12, no. 6, pp. 653–665, Dec. 2008.
- [2] A. C. Rossi, P. J. Brands, and A. P. G. Hoeks, "Automatic localization of intimal and adventitial carotid artery layers with noninvasive ultrasound: A novel algorithm providing scan quality control," *Ultrasound Med. Biol.*, vol. 36, no. 3, pp. 467–479, Mar. 2010.
- [3] F. Molinari et al., "Completely automated multiresolution edge snapper—A new technique for an accurate carotid ultrasound IMT measurement: Clinical validation and benchmarking on a multiinstitutional database," *IEEE Trans. Image Process.*, vol. 21, no. 3, pp. 1211–1222, Mar. 2012.
- [4] Emmanouil G. Sifakis et al., "Robust Carotid Artery Recognition in Longitudinal B-Mode ultrasound images" *IEEE transactions on image processing*, vol. 23, no. 9, september 2014
- [5] F. Faita, V. Gemignani, E. Bianchini, C. Giannarelli, L. Ghiadoni, and M. Demi, "Real-time measurement system for evaluation of the carotid intima-media thickness with a robust edge operator," *J. Ultrasound Med.*, vol. 27, no. 9, pp. 1353–1361, Sep. 2008.
- [6] F. Destrempes, J. Meunier, M.-F. Giroux, G. Soulez, and G. Cloutier, "Segmentation in ultrasonic B-mode images of healthy carotid arteries using mixtures of Nakagami distributions and stochastic optimization," *IEEE Trans. Med. Imag.*, vol. 28, no. 2, pp. 215–29, Feb. 2009.
- [7] R. Rocha, A. Campilho, J. Silva, E. Azevedo, and R. Santos, "Segmentation of the carotid intima-media region in B-mode ultrasound images," *Image Vis. Comput.*, vol. 28, no. 4, pp. 614–625, Apr. 2010.
- [8] R. Rocha, A. Campilho, J. Silva, E. Azevedo, & R. Santos, "Segmentation of ultrasound images of the carotid using RANSAC and cubic splines," *Comput. Methods Programs Biomed.*, vol. 101, no. 1, pp. 94–106, Jan. 2011.
- [9] N. Santhiyakumari, P. Rajendran, M. Madheswar and S. Suresh, "Detection of the intima and media layer thickness of ultrasound common carotid artery image using efficient active contour segmentation technique," *Med. Biol. Eng. Comput.*, vol. 49, no. 11, pp. 1299–310, Nov. 2011.
- [10] W. S. Cleveland, "Robust locally weighted regression and smoothing scatterplots," *J. Amer. Statist. Assoc.*, vol. 74, no. 368, pp. 829–836, Apr. 1979.
- [11] A. W. Bowman and A. Azzalini, *Applied Smoothing Techniques For Data Analysis*. New York ,NY, USA: Oxford Univ. Press, 1997.
- [12] A. M. F. Santos, R. Santos, P. Castro, E. Azevedo, L. Sousa, and J. M. R. S. Tavares, "A novel automatic algorithm for the segmentation of the lumen of the carotid artery in ultrasound mode images," *Expert*

- Syst. Appl., vol. 40, no. 16, pp. 6570–6579, Nov. 2013.
- [13] R. Kazmierski, C. Watala, E. Podsiadly, J. Dorszewska, and W. Kozubski, “Association of atherosclerotic risk factors with carotid adventitial thickness assessed by ultrasonography,” *J. Clin. Ultrasound*, vol. 37, no. 6, pp. 333–341, Jul./Aug. 2009.
- [14] S. Delsanto et al., “Characterization of a completely user-independent algorithm for carotid artery segmentation in 2D ultrasound images,” *IEEE Trans. Instrum. Meas.*, vol. 56, no. 4, pp. 1265–1274, Aug. 2007.
- [15] J. Wan, et al., “Using two methods for recognition common carotid artery of B-mode longitudinal ultrasound image,” in *Proc. IEEE 10th Int. Conf. Signal Process. (ICSP)*, Oct. 2010, pp. 1–4.
- [16] Q. Liang, et al., “A multiscale dynamic programming procedure for boundary detection in ultrasonic artery images,” *IEEE Trans. Med. Imag.*, vol. 19, no. 2, pp. 127–42, Feb. 2000.
- [17] L. Fan, et al., “Ultrasound measurement of brachial flow-mediated vasodilator response,” *IEEE Trans. Med. Imag.*, vol. 19, no. 6, pp. 621–631, Jun. 2000.
- [18] M. A. Fischler and R. C. Bolles, “Random sample consensus: A paradigm for model fitting with applications to image analysis and automated cartography,” *Archive ACM*, vol. 24, no. 6, pp. 381–395, Jun. 1981.
- [19] R. Benes, et al., “Object localization in medical images,” in *Proc. IEEE 34th Int. Conf. Telecommun. Signal Process. (ICTSP)*, Aug. 2011, pp. 559–563.
- [20] A. M. F. Santos, J. M. R. S. Tavares, et al., “Automatic segmentation of the lumen of the carotid artery in ultrasound B-mode images,” *Proc. SPIE*, vol. 8670, pp. 86703I-1–86703I-16, Feb. 2013.
- [21] J. Wikstrand et al., “Methodological considerations of ultrasound investigation of intima-media thickness and lumen diameter,” *J. Internal Med.*, vol. 236, no. 5, pp. 555–559, Nov. 1994.
- [22] Serbia and Montenegro et al., “Image classification based on fuzzy logic” *The International Archives of the Photogrammetry, Remote Sensing and Spatial Information Sciences*, Vol. 34,